High solar energy conversion efficiency and intriguing defect physics are two characteristics of ZnSiP2.

[1]KOTHA SIREESHA,
[2]KOSURI KRISHNA KUMARI,
[3]GADDAM SREEDEVI,
[4]NEELAPUDI RAJESWARI,
Dept.: Humanities & Science
Pallavi Engineering College,
Kuntloor(V),Hayathnagar(M),Hyderabad,R.R.Dist.-501505.

Introduction

Group IV, II–VI, and III–V semiconductors are the most common materials used in optoelectronics because of their tetrahedral coordination. II–IV–V2 (e.g. ZnSiP2) has received less attention for optoelectronic devices than the ternary II–VI analogues such as I–III–VI2 (e.g. CuInSe2), which have been widely studied. 2–9 Many unary and binary semiconductors may be included into the lattice of II–IV–V2-chalcopyrite compounds, as shown in Fig. 1, which displays the wide variety of band gaps and lattice constants that can be found in II–IV–V2 chalcopyrite compounds. As a result, many of the II–IV–V2 compounds are especially suitable for large-scale applications such as photovoltaics since they are generated from very affordable and non-toxic elements (eg. Zn and Mg) (PV). 10–12 Wide range of frequencies There has been very little research on the II–IV–V2 materials, despite the potential for tandem PV, LEDs, photonic circuits, and lasers. 13–15 It has been a challenge to work in tandem PV.

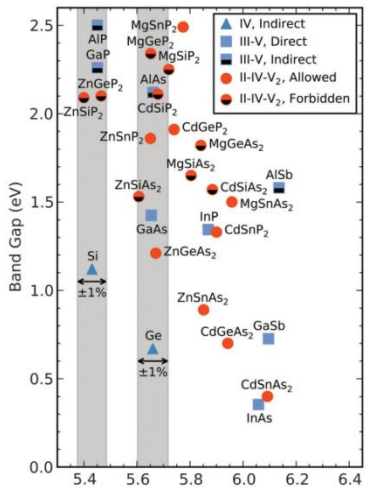

Fig. 1 Theoretically determined band gaps versus lattice constants for some of the more earth abundant II–IV–V2 chalcopyrites. Also shown are III–V materials along with Si and Ge from group IV. The gray vertical bars overlaying Si and Ge highlight materials with similar lattice constant, within 1%

Find materials with large band gaps that can be used in tandems, especially those that are compatible with Si. 16,17 There are two compounds that are particularly interesting as epitaxial top cell materials on a silicon substrate: ZnSiP2 and ZnGeP2. Si PV's supremacy may be leveraged by using these materials as low-cost, readily available top cells (490 percent market share). 18 ZnSiP2 characterization for PV purposes is the subject of this paper. Crystals produced in a flux (usually Zn or Sn) or by halogen-assisted vapour transport have been used since the late 1950s to study ZnSiP2's basic characteristics. 2,11,12,19–36 ZnSiP2 has a very tiny lattice misfit with Si of 0.5 percent, a B2.1 eV band gap, minimum atomic disorder, and is structurally stable at temperatures up to 800 1C, according to the results of these crystals. When ZnSiP2 is doped with n-type elements (Se, Te, In or Ga), p-type crystals (Cu) are formed. 11,19,20,28,31 There has been some characterization done that is directly relevant to tandem silicon photovoltaic cell applications. ZnSiP2 heterojunctions with Si have been suggested and discussed by a number of scientists. 12,25,40,41 Heteroepitaxial crystallisation of Si on ZnSiP2 substrates,39 formation of polycrystalline ZnSiP2 on Si,42 and epitaxial ZnSiP2 on Si via vapor–liquid–solid growth have all been used to illustrate the growth of Si/ZnSiP2 interfaces.

43 Despite the fact that photoconductivity has been shown, no PV devices have been developed. 2,3,44 As the ZnSiP2 has negligible parasitic below-band gap absorption and an excellent index of refraction matching with Si (reflection at the Si/ZnSiP2 interface would be less than 1 percent), the device may be predicted to have strong light transmission from its top cell and into the bottom cell. 37 ZnSiP2 is a suitable material for use as a top cell atop a Si PV

because it is a stable, bipolar dopable, wide band gap semiconductor with a lattice and index of refraction that match Si. It is our goal in this study to address the many unknowns and obstacles associated with ZnSiP2 as a top cell material on Si PV. Using a combination of photoluminescence observations and first principles calculations, we demonstrate that the intrinsic material includes both donor and acceptor defects, and that the energy levels associated with these defects are shallow (B0.1 eV from the corresponding band edge). Antisite faults are the source of these problems. ZnSiP2 shows outstanding photoresponse and a high open circuit voltage (Voc) of 1.3 V in photoelectrochemical (PEC) experiments. We are unaware of any other ZnSiP2 photovoltaic device whose reported voltage is greater than this one, in spite of the fact that this is the first report of its kind. 45–47 A monolithic top cell material based on ZnSiP2 has been created.

Results and discussion

Synthesis and structure

There are ZnSiP2 crystals that are transparent, dark red in hue with diameters up to two millimetres by five millimetres by twenty millimetres long. No. 122 ZnSiP2 crystallises in the I42 percent d space group (a = 5.3986(2) and c = 10.4502(6)) with unit cell dimensions of 5.3986(2) and 10.4502(6). Tables S3–S5 (ESI) provide the findings of the SCXRD structural analysis, which are in good agreement with previously published structural data. 38 The optical characteristics of several chalcopyrites are known to be affected by atomic disorder. 22,48–50 There seems to be no major disorder between the Zn and Si sites 4a and 4b, according on refinements of the SCXRD data. All sites' occupancies remained steady at 1.00(2) (see Table S2, ESI) when occupancies and atomic displacement parameters were allowed to refine. This indicates that all sites are completely occupied. In addition, a structural model was used in which Zn and Si occupied both the 4a and 4b positions. Si occupancy on the 4a site was less than 1.3% using this model, and Zn was not mixed onto the 4b site. This model's statistics are equivalent to those of a model with no mixing of sites. The thermal ellipsoids were virtually spherical as a result of all atomic displacement parameters. Other ternary or quarternary PV materials,48,51–53, have shown that ZnSiP2 favours an atomic structure that is less organised but more stable. 33,

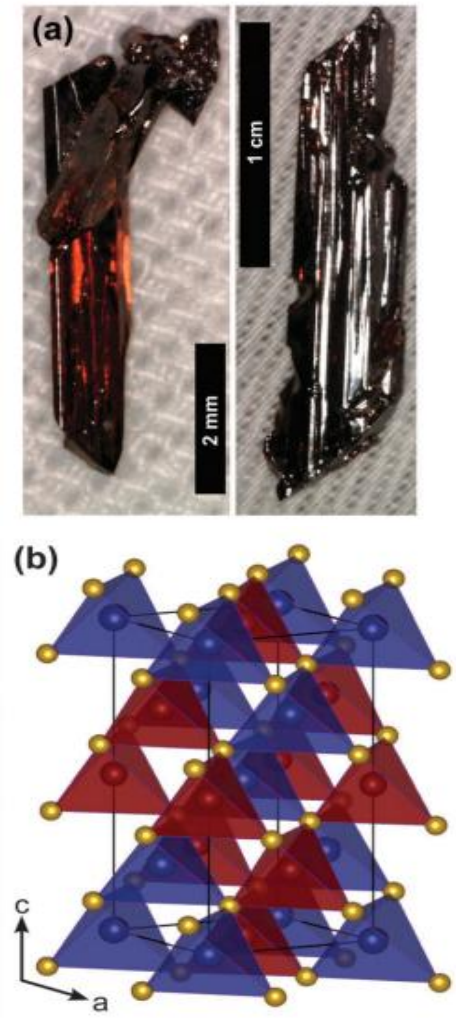

Fig. 2 (a) Photograph of ZnSiP2 single crystals grown in Zn flux. (b) Crystal structure of II–IV–V2 chalcopyrites (I42% d) emphasizing two interlaced networks of corner sharing tetrahedra. In one network, the tetrahedra (red) have a group IV atom at the center and group V atoms on the corners. The second network differs from the first, in that the tetrahedra (blue) are slightly distorted and they have a group II atom at the center

Photoluminescence characterization

ZnSiP2 recombination processes were studied using a combination of photoluminescence (PL) measurements and first-principles calculations (Section 2.4) of intrinsic point defects (vacancies, antisite defects). Measurements of photoluminescence were carried out across a wide temperature range.

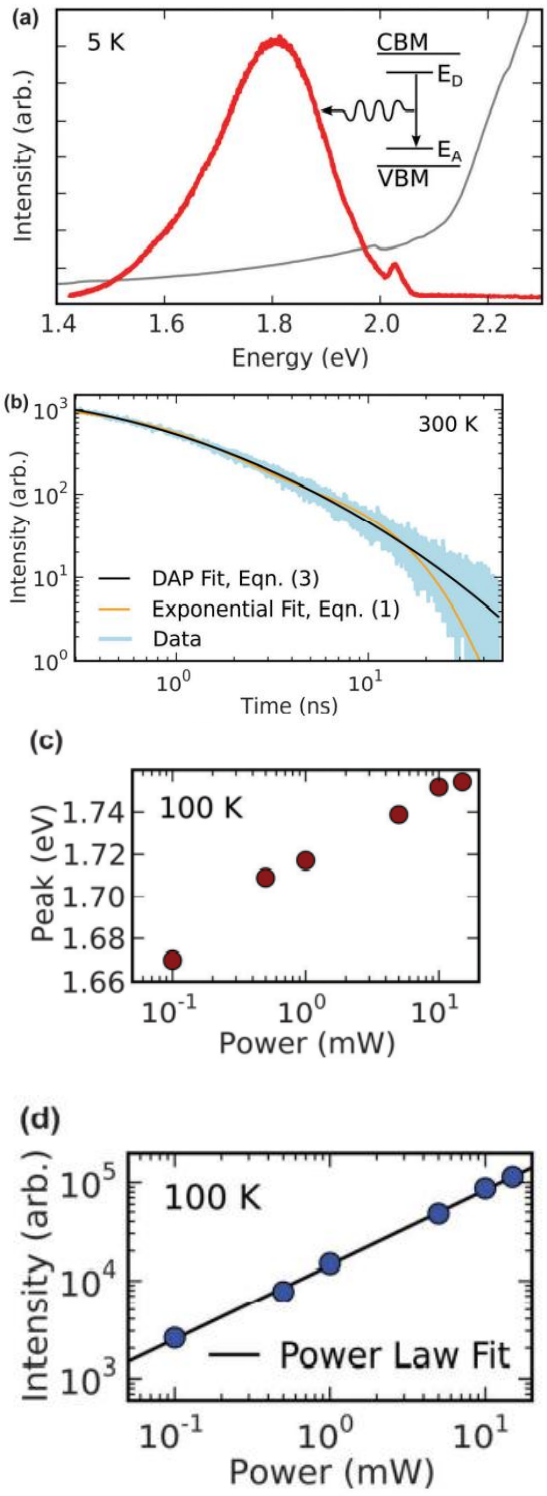

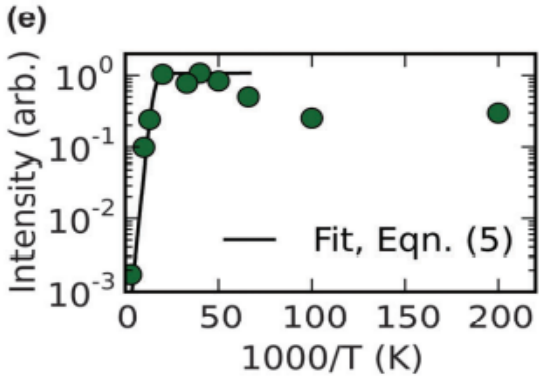

Fig. 3 (a) ZnSiP2 photoluminescence spectrum and absorption edge (grey). The inset graphic indicates the most plausible mechanism for the observed luminescence: donor/acceptor pair transitions. DAP transitions can be seen in the time-dependent 1.8 eV peak, which indicates an excellent carrier lifetime. It is typical of DAP transitions that the power dependency of the 1.8eV peak location exhibits a blue shift. A fit to the data using I(P)p Pk further confirms DAP transitions. (d) The power dependency of the integrated intensity of the 1.8 eV peak. Equation (e) shows that integrated intensity of the 1.8eV peak is temperature dependent, and that the temperature dependence of this peak's integrated intensity corresponds to Eqn (e).Recombination occurs because of the spatially separated electron and hole trapped on donor and acceptor sites having an overlap in their wavefunctions, which is why transitions are the fundamental PL process.56,57 Because of this, the two-process model of PL recombination suggested above is incorrect. 56 For DAP transitions, the recombination rate is assumed to be of the form: r = distance between donorand acceptor.

$$W(r) = W_0 \exp[-2r/a],$$

where W0 is the rate as r - 0 and a is the larger of the donor or acceptor effective Bohr radii.56 The PL intensity as a function of time, t, is proportional to

$$I(t) \propto \exp\left[4\pi N \int_0^\infty (\exp[-W(r)t] - 1) r^2 \mathrm{d}r\right]$$

$$\times 4\pi N \int_0^\infty W(r) \exp[-W(r)t] r^2 \mathrm{d}r,$$

where N is the percentage of the fault that is found in the majority of samples (possibly donors in this case because PEC rectification indicates n-type conductivity). 56 A and N are linked into the nondimensional constant z a3 N, which was used to fit equations (2) and (3) to the data in non-dimensional form (see eqs. (S1) and (S2)), respectively. Figure 3(b) illustrates that, although having fewer free parameters, the final fit is much better than the biexponential fit (orange). z = (2.3 0.3) 10 2 cannot be separated from the contributions of the donor and acceptor, as our theoretical analysis

in Section 2.3 suggests. GaAs's W0 was found to be significantly greater at 8 109 s 1. (3 108 s 1). 58 As shown in Fig. 3(b), DAP transitions are likely the most common recombination mechanism based on eqn (3). However, previous analysis of cathodoluminescence time-dependent at 10 K rather than room temperature found that the recombination was due to bound excitons with sidebands. 59 Temperature-dependent recombination mechanisms may be to blame for this disparity. DAP transitions may be seen in the PL's power reliance. A greater Coulomb interaction between ionised DAPs occurs when the injection level is raised because of the increasing density of excited charge carriers. Following this contact, the energy of the released photons increases:

$$\hbar\omega(r) = E_g - E_A - E_D + \frac{e^2}{r}(\text{cgs}),$$

Here, the transition between donors and acceptors occurs when electrons from the donor ionise the acceptor's nucleus and the acceptor ionises its nucleus at the same time. DAP transitions can be seen in Fig. 3(c), where the peak location shifts to greater energy as the injection volume increases. Finally, the DAP hypothesis may take into account the peak intensity's power dependency (Fig. 3(d)). Models of the type I(P) p Pk were used to fit the experimental data. P represents the excitation power and k the exponent. The average k was 0.72, with a standard deviation of 0.12, for the nine temperatures at which power-dependent data was gathered. Radiative recombination is mostly caused by free-to-bound or DAP transitions with k o 1, as seen by the peak intensity's power dependency. 60 Additionally, the activation energy of the donor may be determined through PL data analysis (the material is n-type, as shown in Section 2.4). According to Fig. 3(e), when the temperature is reduced to 25 K, the integrated intensity rises dramatically. The intensity of the PL dropped and seemed to saturate below 25 K. Temperatures greater than 25 K were found to be suitable for

$$I(T) \propto \frac{1}{1 + \alpha e^{(E_D/k_B T)}},$$

where kB is Boltzmann's constant, and T is the temperature, and an is a process rate parameter. 61 These six temperature-dependent data sets yielded an activation energy of ED=58 16 meV, which is shallow and consistent with earlier results, and is in accord with these findings. 59,62 DAP recombination is shown by the time and power dependency of the PL intensity and the peak location. A shallow donor level is predicted by the temperature dependence of the PL intensity, which is in line with the high Voc values reported in the PEC characterization, since there were no deep-level defects discovered in the PL.

2.3 Identification of potential intrinsic defects

First-principles density functional theory (DFT) simulations were used to discover probable point defects in ZnSiP2 that operate as donors and acceptors in order to better understand charge carrier recombination. The stability map in chemical potential space was generated by estimating the enthalpies of formation of known Zn–Si–P phases (Fig. 4a). 63 Figure 4(b) shows the enthalpy of production of intrinsic defects in the ZnSiP2 area of stability of this chemical potential space, as well as the related density of states (DOS) for relevant defects. Calculations were made on the formation enthalpies (DHD,q) of seven different point defect types (three vacancies and four antisite defects) in seven different charge states (3 through 3+; 4 and 4+ were also examined for VSi) based on Zn, Si, and P chemical potentials and Fermi level, in order to determine the formation enthalpies (DHD,q) of these point defect types (EF). Previous EPR experiments have showed evidence of Zn and P vacancies as well as Si on Zn antisite defects64,65; however, these are the first calculations that indicate plausible point defects for ZnSiP2 as a function of chemical potential.64,65 Fitted Elemental-Phase Reference Energies (FERE) were used to determine the Zn–Si–P phase diagram under normal conditions (a). In this chemical potential phase space, 63 ZnSiP2 fills a considerable portion of it, implying a wide range of synthesis conditions. Compounds like SiP and Zn3P2 compete with Zn and P elements in this phase, as well as binary compounds like ZnP2.

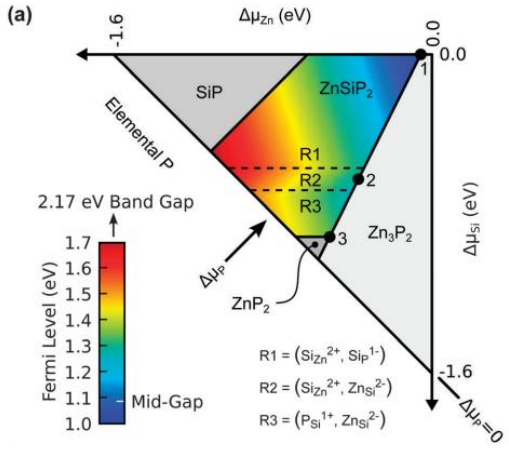

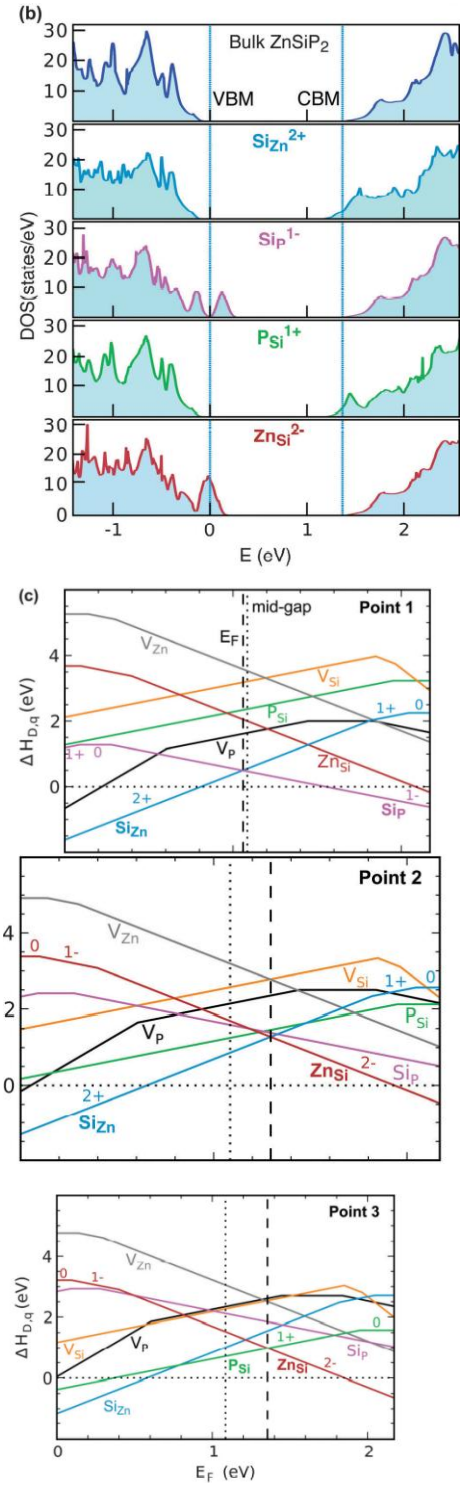

Chemical potential phase space phase diagram of a Zn–Si–P system (Fig. 4a). Zn-rich flux growth conditions are likely to fall somewhere between points 1 and 3. A heat map of the Fermi level (EF) is also displayed, which runs from point 1 at the mid-gap to B1.7 eV above the valence band peak. Different donor–acceptor couples predominate in R1, R2, and R3 sections of the chemical potential phase space. Phase diagram points 1, 2, and 3 are shown on the defect formation enthalpies of 7 point defects (vacancies and antisites) in all conceivable charge states, with q ranging from 4 to 4+. (a). Vertical dashed lines indicate the Fermi level. line along with mid-gap which is shown as a dotted vertical line, with the Fermi level-defining flaws highlighted in bold. See Fig. S1 (ESI) for further information on all the charge states of each point defect. Without defects, and ZnSiP2 with four essential native point defects (SiZn2+, Sip 1, and PSI1+1): (c) The density of states (DOS) of the two materials. There is no indication of mid-gap states that may trap carriers and negatively impact Voc in the corresponding defect states, which are shallow and appear as shoulders of the relevant band edges.

There are three unique regimes (designated R1, R2, and R3) with differing lowest DHD,q defect pairings in the single phase area where ZnSiP2 is stable. SiZn2+ and SiP 1 in Region 1, PSi 1+ and ZnSi 2 in Region 2, and SiZn2+ and ZnSi 2 in Region 3 are the major DAPs that determine the Fermi level. Figure 4 depicts the Fermi levels (EF) as dashed vertical lines (b). Zn-rich, Si-poor, and P-poor conditions were used to generate the ZnSiP2 crystals. In Fig. 4, the line linking points 1 and 2 and 3 shows the most probable location of these favourable development circumstances (a). Defect enthalpies and concentrations were studied at these sites, which are located in R1, R2, and R3 in Figure 4 and relate to the respective areas (a). Fig. 4(b) shows DHD,q as a function of EF for the point defects studied, where the formation enthalpy of the lowest-energy DAP is given in bold for each of the three points. Defect concentrations may be approximated to a first-order precision from

$$[C] = [S]e^{-\frac{\Delta H_{D,q}}{k_B T}},$$

The Boltzmann constant kB, the temperature at which the defects occur, and the chemical potentials associated with a given location in Fig. 4(a) and the accompanying Fermi level are used to calculate the DHD,q for each point. Zn flux crystallisation happens when the temperature of the Zn flux progressively cools (B2 1C h 1) from 1000 to 500 1C before quickly cooling down to room temperature; this results in reduced limits on what may be seen

experimentally. Table 1 shows the calculated DAPs and their corresponding concentrations. Defect-free ZnSiP2 and ZnSiP2 with one of the four significant flaws are shown in Fig. 4's density of states (DOS) (c). The conduction band minimum (CBM) and the valence band maximum (VBM) are where the shallow donor and acceptor states appear as shoulders. In any event, there is no evidence for mid-gap states. Extrinsic impurity (Cu) doping has been implicated in previous investigations as the cause of a high acceptor level, B0.7 eV above the VBM. In ZnSiP2, DAP antisite defects seem to be the most common recombination mechanism, as shown by PL measurements and theoretical defect predictions. ZnSiP2 is likely to be intrinsic, or moderately n-type, throughout a broad range of synthesis conditions because of these DAP defects. The donor level was determined to be shallow: B58 meV below the CBM, based on an analysis of the temperature dependence of the PL intensity. Based on their DOS, the most common flaws in the calculations were determined to be located at shallow depths. Findings from this study show that ZnSiP2 PV devices are defect-tolerant and should have a high Voc, which is consistent with Section 2.4's PEC results.

Conclusions

ZnSiP2 has the potential to be a high-quality photovoltaic top cell material, as shown by a combination of photoeletrochemical (PEC) characterisation, photoluminescence (PL) tests, and theoretical intrinsic defect calculations. The open circuit voltage was found to be 1.3 eV, confirming the absence of deep-level flaws. Both shallow donor–acceptor pairings and deep-level faults were found by PL. The stability window in Zn–Si–P chemical potential space has shallow antisite defects as the dominating defects, according to theoretical defect calculations. It is also expected that ZnSiP2 is significantly n-type over this whole chemical potential area. As a result, this material has a high degree of stability and flaw tolerance inherent to it. ZnSiP2 shows tremendous promise as a top cell on Si because of its abundance, defect tolerance, high voltage potential, and broad phase-stability window in this initial research.

References

[1] M. A. Green, J. Mater. Sci.: Mater. Electron., 2007, 18, 15–19.

[2] G. Ku¨hnel, W. Siegel and E. Ziegler, Phys. Status Solidi A, 1975, 30, K25–K27.

[3] T. Shirakawa, K. Okamura and J. Nakai, Phys. Lett. A, 1979, 73, 442–444.

[4] H. Shin and P. Ajmera, Mater. Lett., 1987, 5, 211–214.

[5] H. Shin and P. Ajmera, Mater. Lett., 1989, 8, 464–467.

[6] Y.-C. Wen and B. A. Parkinson, J. Phys. Chem. B, 1997, 101, 2659–2662.

[7] T. J. Peshek, L. Zhang, R. K. Singh, Z. Tang, M. Vahidi, B. To, T. J. Coutts, T. A. Gessert, N. Newman and M. van Schilfgaarde, Progress in Photovoltaics: Research and Applications, 2013, 21, 906–917.

[8] G. Xing, K. Bachmann, J. Posthill and M. Timmons, J. Cryst. Growth, 1991, 113, 113–119.

[9] S. G. Choi, M. van Schilfgaarde, D. E. Aspnes, A. G. Norman, J. M. Olson, T. J. Peshek and D. H. Levi, Phys. Rev. B: Condens. Matter Mater. Phys., 2011, 83, 235210.

[10] (a) C. L. Goodman, Nature, 1957, 179, 828–829; (b) A. N. Fioretti, A. Zakutayev, H. Moutinho, C. Melamed, J. D. Perkins, A. G. Norman, M. Al-Jassim, E. S. Toberer and A. C. Tamboli, J. Mater. Chem. C, 2015, 3, 11017–11028.

[11] A. Sping-Thorpe and B. Pamplin, J. Cryst. Growth, 1968, 3, 313–316.

[12] V. D. Prochukhan and V. R. Yu, Soviet Physics: Semiconductors, 1977, 12, 129–132.

[13] H. Morkoc, S. Strite, G. Gao, M. Lin, B. Sverdlov and M. Burns, J. Appl. Phys., 1994, 76, 1363–1398.

[14] M. A. Green, Progress in Photovoltaics: Research and Applications, 2001, 9, 123–135.

[15] R. Soref, IEEE J. Sel. Top. Quantum Electron., 2006, 12, 1678–1687.

[16] N. Jain and M. K. Hudait, Energy Harvesting and Systems, 2014, 1, 121–145.

[17] C. D. Bailie, M. G. Christoforo, J. P. Mailoa, A. R. Bowring, E. L. Unger, W. H. Nguyen, J. Burschka, N. Pellet, J. Z. Lee, M. Gratzel, R. Noufi, T. Buonassisi, A. Salleo and M. D. McGehee, Energy Environ. Sci., 2015, 8, 956–963.

[18] Fraunhofer ISE, Photovoltaics Report, 28 July 2014, p. 18, http://www.webcitation.org/6SFRTUaBS, Achived 31 August, 2014.

[19] A. Springthorpe and R. Monk, Phys. Status Solidi A, 1970, 1, K9–K12.

[20] E. Ziegler, W. Siegel and G. Kuehnel, Phys. Status Solidi A, 1973, 18, 483–487. 21 W. Siegel and E. Ziegler, Phys. Status Solidi A, 1974, 21, 639–647.